Title	Evaluation of neutron nuclear data on tantalum isotopes
Author(s)	Shibata Keiichi
Citation	Journal of Nuclear Science and Technology,53(7),p.957-967
Text Version	Author's Post-print
URL	https://jopss.jaea.go.jp/search/servlet/search?5051596
DOI	https://doi.org/10.1080/00223131.2015.1083492
Right	This is an Accepted Manuscript of an article published by Taylor & Francis in Journal of Nuclear Science and Technology on July 2016, available online: http://www.tandfonline.com/10.1080/00223131.2015.1083492.”

Evaluation of neutron nuclear data on tantalum isotopes

Keiichi Shibata*

Nuclear Data Center, Japan Atomic Energy Agency, Tokai-mura, Ibaraki 319-1195, Japan

Neutron nuclear data on four isotopes of tantalum have been evaluated for the next version of Japanese Evaluated Nuclear Data Library general-purpose file in the energy region from 10^{-5} eV to 20 MeV. Unresolved resonance parameters were obtained by fitting to the total and capture cross sections calculated from nuclear models, while resolved resonance parameters were selected from experimental data. A statistical model code was applied to evaluate cross sections above the resolved resonance region. Compound, pre-equilibrium and direct-reaction processes were considered for cross-section calculation. Coupled-channel optical model parameters were employed for the interaction between neutrons and nuclei. Giant-dipole and pygmy resonance parameters for E1 γ-ray transition from tantalum isotopes were determined so as to reproduce measured γ-ray spectrum for ^{181}Ta. The present results reproduce experimental data very well. The evaluated data are compiled into ENDF-formatted data files.

Keywords: neutron nuclear data; evaluation; tantalum isotopes; cross section; JENDL; resonance parameter; optical model; statistical model

*Corresponding author. Email: shibata.keiichi@jaea.go.jp

1. Introduction

Nuclear data are required for nuclear science and engineering. Especially, neutron-induced reaction data are important for nuclear energy applications. Japanese Evaluated Nuclear Data Libraries (JENDLs) have been developed by the Japan Atomic Energy Agency (JAEA) since 1977. The fourth version of the general-purpose file, JENDL-4.0, was released[1] in 2010. JENDL-4.0 contains neutron-induced reaction data for 406 nuclides, and its good performance was proved[2] by benchmarking. However, in the JENDL-4.0 evaluations, tantalum data were not fully examined due to the deadline of the release. Tantalum is regarded as a control-rod material for lead-bismuth cooled fast reactors, and so its neutron data are important. Moreover, neutron-induced activation cross sections of tantalum are needed[3] for the decommissioning of light-water reactors.

The data on ^{181}Ta were evaluated for JENDL-3.0[4] in 1987. These data were essentially carried over to JENDL-4.0 with minor modifications, although other isotopes were not considered. Under such circumstances, the present work was undertaken to improve the evaluated data on ^{181}Ta by considering the latest knowledge on experimental and theoretical nuclear physics. In addition to ^{181}Ta, the data on ^{179,180m,182}Ta were newly evaluated. Evaluated are the total, elastic and inelastic scattering, (n, γ), (n, p), (n, d), (n, t), $(n,^3 He)$, (n, α), (n, np), (n, nd), $(n, n\alpha)$, $(n, 2n)$, $(n, 3n)$, $(n, 2np)$ reaction cross sections, the angular distributions of elastically and inelastically scattered neutrons and the energy distributions of emitted particles and γ-rays in the energy region from 10^{-5} eV to 20 MeV. The Q-values of the reactions were calculated from the mass table AME2012[5], and are listed in **Table 1**, together with abundances[6] and half-lives[7].

[Table 1 about here.]

This paper presents how the evaluation was performed. Section 2 deals with the resonance region. In Section 3, the computational methods and procedures above the resonance region are described. Comparisons of the evaluated results with the experimental and existing evaluated data are made in Section 4. Finally, Section 5 summarises the conclusion.

2. Resonance region

The resolved and unresolved resonance regions are listed in **Table 2** for each target nucleus. In principle, resolved resonance parameters (RRPs) are obtained from the analyses of experimental data. RRPs are unavailable for ^{179}Ta, since no measurements have been published in the resonance region. Constant and $1/v$ energy dependences are assumed for the elastic scattering and capture cross sections of ^{179}Ta, respectively, up to the lower limit of unresolved resonance region. Normalisation of the cross sections is done at thermal energy. The thermal scattering cross section was calculated as $4\pi R^2$, where R stands for the scattering radius that can be estimated from nuclear model calculations in the higher energy region. On the other hand, the thermal capture cross section of ^{179}Ta was estimated from the activation data measured by Schumann and Käppeler[8] combined with the isomeric ratio calculated from nuclear models. The RRPs of ^{180m}Ta and ^{182}Ta were taken from the work of Harvey et al.[9] and Stokes et al.[10], respectively, while those of ^{181}Ta remain unchanged from JENDL-4.0. As for ^{181}Ta, the latest transmission data of Meaze et al.[11] were not adopted in the present work, since their radiation widths were extremely large for several resonances as compared with other measurements. The lowest resonances were added at 0.2 eV and -20 eV for ^{180m}Ta and ^{182}Ta, respectively, by considering the compilation of Mughabghab[12]. The thermal capture and elastic scattering cross sections are listed in **Table 3**, where the capture and elastic scattering cross sections are given at 300 K and 0 K, respectively, in order to compare with the values recommended by Mughabghab.

The ASREP code[13] was used to determine the unresolved resonance parameters (URPs) by fitting to the total and capture cross sections calculated with the nuclear models which will be described in Section 3. The URPs obtained are used only for self-shielding calculations, since the pointwise cross sections are given in the evaluated data files. As an example, the cross sections of ^{182}Ta reconstructed from the URPs are compared with the total and capture cross sections calculated from the nuclear models in **Figure 1**. In the parameter fitting with the ASREP code, 10% uncertainties in the nuclear model calculations were assumed. The reconstructed cross sections reproduce the nuclear model calculations very well.

[Table 2 about here.]

[Table 3 about here.]

[Figure 1 about here.]

3. Computational methods and procedures above resonance region

3.1. Nuclear models

The CCONE code (Version 0.8.4)[14] was used for calculating the neutron-induced reaction cross sections of tantalum isotopes. The code is based on the spherical and coupled-channel optical models, the two-component exciton pre-equilibrium model, the distorted-wave Born approximation (DWBA) and the multi-step statistical model. In order to simulate the direct and semi-direct effects on the radiative capture reaction, the pre-equilibrium capture was considered by using the γ-ray emission rate of Akkermans and Gruppelaar[15] extended to the two-component exciton pre-equilibrium model.

3.2. Parameter determination

3.2.1. Optical-model potentials

As for neutrons, we employed the global optical-model parameters obtained by Kunieda et al.[16] using the coupled-channel method based on the rigid rotor model[17]. The potential $V(r)$ is defined as

$$\begin{aligned} V(r) &= -V_R f_R(r) - i\left\{W_V f_V(r) - 4W_D a_D \frac{d}{dr} f_D(r)\right\} \\ &+ \left(\frac{\hbar}{m_\pi c}\right)^2 (V_{SO} + iW_{SO}) \frac{1}{r}\frac{d}{dr} f_{SO}(r) \boldsymbol{L}\cdot\boldsymbol{\sigma}, \end{aligned} \quad (1)$$

where $\boldsymbol{L}$ and $\boldsymbol{\sigma}$ are the orbital angular momentum and the Pauli matrix, respectively. The form factor $f_i(r)$ is of a Woods-Saxon shape, i.e.,

$$f_i(r) = \frac{1}{1 + exp\{(r - R_i)/a_i\}}, \quad i = R, D, V, SO, \quad (2)$$

where R_i is written as

$$R_i = R_i^0 \left[1 + \sum_{l=2,4,\ldots} \beta_l Y_l^0(\theta)\right]. \quad (3)$$

The angle θ refers to the body-fixed system, and Y_l^0 and β_l denote spherical harmonics and a deformation parameter, respectively. The potential depths are given as follows:

$$\begin{aligned} V_R &= (V_R^0 + V_R^1 E^\dagger + V_R^2 E^{\dagger 2} + V_R^3 E^{\dagger 3} + V_R^{DISP} exp(-\lambda_R E^\dagger)) \\ &\times \left[1 - \frac{1}{V_R^0 + V_R^{DISP}} C_{viso} \frac{N-Z}{A}\right], \end{aligned} \quad (4)$$

$$\begin{aligned} W_D &= \left[W_D^{DISP} - C_{wiso}\frac{N-Z}{A}\right] exp(-\lambda_D E^\dagger) \\ &\times \frac{E^{\dagger 2}}{E^{\dagger 2} + WID_D^2}, \end{aligned} \quad (5)$$

$$W_V = W_V^{DISP} \frac{E^{\dagger 2}}{E^{\dagger 2} + WID_V^2}, \quad (6)$$

$$V_{SO} = V_{SO}^0 exp(-\lambda_{SO} E^\dagger), \quad (7)$$

$$W_{SO} = W_{SO}^{DISP} \frac{E^{\dagger 2}}{E^{\dagger 2} + WID_{SO}^2}, \quad (8)$$

where Z, A, and N are the atomic number and mass number of a target and $N = A - Z$, respectively. The symbol $E^\dagger$ is the incident-neutron energy (E) relative to the Fermi one (E_f), i.e, $E^\dagger = E - E_f$. The Fermi energy E_f is calculated from neutron-separation energies (S_n) of target and compound nuclei such as $E_f = -\{(S_n(Z, A) + S_n(Z, A+1)\}/2$.

From the neutron potentials, transmission coefficients are obtained together with total cross sections, shape-elastic scattering cross sections and the direct-reaction components of inelastic scattering cross sections for the CCONE calculation.

The parameters required in Eqs. (2)–(8) are listed in **Table 4**, and the coupling schemes and deformation parameters are given in **Table 5**. The deformation parameters were originally taken from the work of Koura et al.[18] The calculated total cross section of elemental Ta is shown in **Figure 2** together with experimental data and the spherical optical model calculations using the parameters of Koning and Delaroche[19]. In order to give a better fit to experimental data, the values of W_D^{DISP} and W_V^{DISP} were adjusted together with the β_4 value for ^{181}Ta, while the rest of the parameters remain unchanged from the original ones[16]. It is found from Figure 2 that the present calculations reproduce measured data better than those using the parameters of Koning and Delaroche. Concerning charged-particles, used were the spherical parameters of Koning and Delaroche[19] for protons, those of Lohr and Haeberli[20] for deuterons, those of Becchetti and Greenlees[21] for tritons and ^{3}He, and those of Lemos[22] modified by Arthur and Young[23] for α-particles. The transmission coefficients, which are required by CCONE to calculate charged-particle emission, were obtained from the charged-particle parameters.

[Table 4 about here.]

[Table 5 about here.]

[Figure 2 about here.]

3.2.2. Discrete levels and level density

In the calculation, it was necessary to input the discrete levels and level density parameters for 19 nuclei, i.e., $^{177-183}$Ta, $^{177-182}$Hf, and $^{175-180}$Lu. The discrete levels were taken from the reference input parameters library RIPL-3[24].

Concerning the level density, the composite formula of Gilbert and Cameron[25] was used in the present work. In the region of low excitation energy E, the level density is described by the constant temperature formula ρ_T, namely,

$$\rho_T(E) = \frac{1}{T} exp\Big(\frac{E - E_0}{T}\Big). \tag{9}$$

On the other hand, the a parameter, which characterises the Fermi-gas part of level density ρ_F, is defined as

$$a(U) = a(*) \left[1 + \frac{E_{sh}}{U}(1 - e^{-\gamma U})\right], \tag{10}$$

where E_{sh} is the shell correction energy and γ a damping factor. The damping factor is given by $\gamma = 0.40 A^{-1/3}\mathrm{MeV}^{-1}$. The energy U is expressed by E and the pairing energy Δ, i.e., $U = E - \Delta$. In the above equations, the values of $a(*)$ and Δ were taken from the work of Mengoni and Nakajima[26]. The shell correction energy E_{sh} is calculated as the difference between the experimental mass[5] and the theoretical mass[27]. The two parameters T and E_0 were determined so as to connect ρ_F and ρ_T smoothly at an appropriate matching energy E_m. The parameters used in this work are listed in **Table 6** for individual nuclei, together with the energies of the highest discrete levels $E_{level}^{highest}$.

[Table 6 about here.]

3.2.3. Gamma-ray transition

The γ-ray transmission coefficients are related to the photoabsorption cross sections by the detailed balance. The photoabsorption cross section is usually approximated by various Lorentzian shapes. In the present calculation, the shape was determined by comparing with the gamma-ray spectrum measured by Voignier et al.[28, 29] at 500 keV. As for the E1 radiation, two giant-dipole resonance (GDR) terms and a pygmy resonance (PR) term were needed to reproduce the spectra. An enhanced generalised Lorentzian (EGLO), which was proposed by Kopecky et al.[30], was used for these terms. The resonance energy ($E_{0,i}$), resonance width ($\Gamma_{0,i}$) and peak cross section ($\sigma_{0,i}$) were fixed for all tantalum isotopes, and they are given in **Table 7**. The calculated γ-ray spectrum is compared with the data measured by Voignier et al. at an angle of 90 degrees in **Figure 3**, where the measurements are multiplied by 4π. The agreement between the calculation and the experiment becomes satisfactory by considering the pygmy term, as was indicated by Igashira et al.[31] For other nuclei, two-component GDR parameters for EGLO are determined from the RIPL-3[24] prescription for deformed nuclei. They are explicitly given as follows:

$$E_{0,1} = \frac{E_0}{b_0}\frac{[1 - 1.51 \times 10^{-2}(a_0^2 - b_0^2)]}{[0.911\frac{a_0}{b_0} + 0.089]} \quad \text{MeV}, \tag{11}$$

$$E_{0,2} = \frac{E_0}{b_0}[1 - 1.51 \times 10^{-2}(a_0^2 - b_0^2)] \quad \text{MeV}, \tag{12}$$

$$\Gamma_{0,1} = 0.026E_{0,1}^{1.91} \quad \text{MeV}, \tag{13}$$

$$\Gamma_{0,2} = 0.026E_{0,2}^{1.91} \quad \text{MeV}, \tag{14}$$

$$\sigma_{0,1} = \sigma_0/3 \quad \text{mb}, \tag{15}$$

$$\sigma_{0,2} = 2\sigma_0/3 \quad \text{mb}, \tag{16}$$

where the systematics of E_0 and σ_0 are given[32] by

$$E_0 = 31.2A^{-1/3} + 20.6A^{-1/6} \quad \text{MeV}, \tag{17}$$

$$\sigma_0 = 1.2 \times 120NZ/(0.026E_0^{1.91}A\pi) \quad \text{mb}. \tag{18}$$

Using the quadrupole deformation parameter β_2 tabulated by Möller et al.[33], the remaining quantities needed to estimate Eqs. (11) and (12) are obtained from

$$\alpha_2 = \sqrt{\frac{5}{4\pi}}\beta_2, \tag{19}$$

$$\lambda = \left(1 + \frac{3}{5}\alpha_2^2 + \frac{2}{35}\alpha_2^3\right)^{1/3}, \tag{20}$$

$$a_0 = (1 + \alpha_2)/\lambda, \tag{21}$$

$$b_0 = (1 - 0.5\alpha_2)/\lambda. \tag{22}$$

The standard Lorentzian (SLO) form was used to describe the M1 and E2 radiations for which the parameters were taken from the work of Kopecky and Uhl.[34]

In cases where measured capture cross sections are available in the keV region, the γ-ray strength functions are renormalised so that the calculated cross sections reproduce these data. The s-wave γ-ray strength functions are compared in **Table 8** with the values recommended by Mughabghab[12]. The values of ^{181,182}Ta were obtained after renormalisation using measurements. Although the value of ^{180}Ta seems large as compared with the others, it would not be possible to judge whether the present calculation is reasonable without measured cross sections in the keV region.

[Table 7 about here.]

[Table 8 about here.]

[Figure 3 about here.]

3.2.4. Pre-equilibrium parameters

The Version 0.8.4 of CCONE incorporates pre-equilibrium process for the (n,γ) and first-step binary reactions such as (n,n'), (n,p), (n,d), (n,t), $(n,^3He)$ and (n,α). In the two-exciton pre-equilibrium formalism, the single-particle state densities for protons and neutrons in a residual nucleus are described[35] by

$$g_\pi = \frac{C_0 Z}{15} \quad \mathrm{MeV}^{-1}, \tag{23}$$

$$g_\nu = \frac{C_0 N}{15} \quad \mathrm{MeV}^{-1}, \tag{24}$$

respectively. The parameter C_0, of which the default value is unity, is changed so that the calculations reproduce measured neutron and proton emission data such as $(n,2n)$ and (n,p) in the present work. The $(n,2n)$ reaction is a ternary reaction, which proceeds from (n,n') by sequential decay in the framework of the multi-step statistical model. Hence, the $(n,2n)$ cross section is sensitive to C_0 for the residual nucleus in the (n,n')

reaction. More experimental data are available for $(n, 2n)$ than for (n, n') in the nuclides presently concerned. In addition to the C_0's, the pre-equilibrium parameters for complex-particle emission[36] were determined, i.e., those for the deuteron pickup reaction from the ^{181}Ta(n, t) reaction and those for the ^{3}He pickup and the α knockout reactions from the ^{181}Ta(n, α) reaction. These parameters for the complex particles were used for all tantalum targets. The pre-equilibrium parameters used are listed in **Table 9**, where C_0's are given only for the residual nuclei in the (n, n') and (n, p) reactions, and are assumed to be unity for those in the other first-step binary reactions.

[Table 9 about here.]

4. Comparison with experimental data and other evaluated data in the fast-neutron region

Comparisons are made with experimental data and other evaluated data. The experimental data are taken from the EXFOR database[37] that is compiled by the international data centres such as the IAEA Nuclear Data Section, the OECD NEA Data Bank, and the National Nuclear Data Center at the Brookhaven National Laboratory. As for the general-purpose evaluated nuclear data, there exist three major libraries, namely JENDL-4.0[1], ENDF/B-VII.1[38] and JEFF-3.2[39]. Concerning tantalum, JENDL-4.0 contains the data only for ^{181}Ta, while ENDF/B-VII.1 and JEFF-3.2 have the data of ^{180g,181,182}Ta and ^{180m,181,182}Ta, respectively. These general-purpose libraries do not contain activation cross sections leading to the ground or isomeric state. The activation cross-section files JENDL/A-96[40] and JEFF-3.1/A[41] are used for comparison with such activation data. We do not discuss most of the reactions where experimental data are unavailable, since it is difficult to judge whether the present evaluation is reasonable without measurements.

The capture cross section of ^{180m}Ta is illustrated in **Figure 4**. The present evaluation reproduces the data measured by Wisshak et al.[42] very well, while the JEFF-3.2

evaluation is systematically larger than the measurements. **Figure 5** shows the capture cross sections of ^{181}Ta. It is found from the figure that the present evaluation is in good agreement with the measured data. The JENDL-4.0 evaluation is inconsistent with the experimental data at 14 MeV, which is due to the ignorance of the direct and semi-direct effects in this region. An enhancement of ENDF/B-VII.1, which is seen in the 1- to 3-MeV region, is not justified by available experimental data. The residual nucleus ^{182}Ta has two meta-stable states, i.e., J^{π} = 5^{+} with $T_{1/2}$ = 283 ms for E_x = 16.3 keV and J^{π} = 10^{-} with $T_{1/2}$ = 15.84 m for E_x = 519.6 keV in the incident energy region presently concerned. The partial activation cross sections are compared in **Figures 6** and **7** with measurements and other evaluated data. The measured ground-state (GS) ($J^{\pi} = 3^{-}$, $T_{1/2}$ = 114.74 d) production in Figure 6 includes the contribution from the 5^{+} state of which half-life is considerably smaller than that of GS. It should be noted that the 5^{+} state is not regarded as meta stable in JENDL/A-96 and so its contribution is automatically included in the GS production. The calculated isomeric ratio was slightly modified below 60 keV so as to reproduce the thermal ^{181}Ta$(n,\gamma)^{182m2}$Ta cross section recommended by Mughabghab[12]. The presently evaluated activation cross sections agree with available experimental data, although the data of Cox[43] are systematically larger than all the evaluated data for ^{181}Ta$(n,\gamma)^{182m2}$Ta.

Figures 8 and **9** show the total and partial $(n,2n)$ cross sections of ^{181}Ta, respectively. The data of Frehaut et al.[44] were renormalised by a factor of 1.078 that was derived by Vonach et al.[45] The experimental data on the total and partial $(n,2n)$ cross sections are well reproduced by the present evaluation, although the total 14.1-MeV $(n,2n)$ cross section measured by Ashby et al.[46] (2.64 ± 0.20 b), which would be located outside Figure 8, is much larger than the existing evaluated data. All the evaluations are almost consistent with the ^{181}Ta$(n,3n)^{179}$Ta cross section measured by Veeser et al.[47], as seen in **Figure 10**.

The (n,p), (n,t), and (n,α) reaction cross sections of ^{181}Ta are illustrated in **Figures 11**, **12**, and **13**, respectively. The measured cross sections are well reproduced by the presently evaluated cross sections for all reactions, while the ENDF/B-VII.1 evaluation is relatively large. The JEFF-3.2 evaluation is consistent with the present work. Moreover, it is found from **Figure 14** that the bulk of the experimental data on the ^{181}Ta$(n,np+d)^{180m}$Hf reaction are reproduced by the present evaluation, although the 13.5-MeV cross section measured by Luo et al.[48] is larger than the present and JEFF-3.1/A evaluations.

Angular distributions of neutrons elastically scattered from ^{181}Ta are shown in **Figure 15**. All the calculations include the contributions of the neutrons inelastically scattered from the first and second excited states ($E_x = 6.2$ and 136.4 keV, respectively), since we believe that such inelastic neutrons were not fully corrected for in the measurements. The present evaluation agrees with the measurements in the region above 10 MeV. This fact proves the reliability of the neutron optical model parameters presently used.

Angle-integrated neutron emission spectra for ^{181}Ta are shown in **Figure 16**. As in the case[49] of ^{75}As, we assumed a pseudo-resonance at an excitation energy of 2.1 MeV for ^{181}Ta, which can substitute for the missing collective enhancement phenomenologically. The cross section for the resonance was calculated by DWBA using the neutron potential parameters mentioned in Sect. 3 with $\beta_2 = 0.12$, and it was smeared by a normal distribution with a standard deviation of 2.1 MeV. The present and JEFF-3.2 evaluations reproduce the measured spectra well. On the other hand, the JENDL-4.0 and ENDF/B-VII.1 evaluations are systematically smaller than the measured spectra in the energy region below the elastic peaks, where the pre-equilibrium effect is significant. The pre-equilibrium reaction yields forward-peaking angular distributions of continuous-energy neutrons as seen in **Figure 17**. Such forward-peaking distributions are not given by JENDL-4.0.

[Figure 4 about here.]

[Figure 5 about here.]

[Figure 6 about here.]

[Figure 7 about here.]

[Figure 8 about here.]

[Figure 9 about here.]

[Figure 10 about here.]

[Figure 11 about here.]

[Figure 12 about here.]

[Figure 13 about here.]

[Figure 14 about here.]

[Figure 15 about here.]

[Figure 16 about here.]

[Figure 17 about here.]

5. Concluding remarks

The neutron nuclear data on tantalum isotopes were evaluated in the energy region from 10^{-5} eV to 20 MeV. The RRPs of ^{180m,182}Ta were taken from experimental data, while those of ^{181}Ta remain unchanged from JENDL-4.0. In the low-energy region, the $1/v$ behaviour was assumed for the capture cross section of ^{179}Ta for which RRPs were unavailable. The URPs were obtained for self-shielding calculations by fitting to the total and capture cross sections calculated from the nuclear models.

The statistical-model code CCONE was applied to the calculation of fast-neutron cross sections. The neutron transmission coefficients were obtained by the coupled-channel method, together with the total cross sections, the shape-elastic scattering cross sections and the direct-reaction components of the inelastic scattering cross sections. The neutron potentials were found to be reliable by comparing with the measured total cross sections.

The GDR and PR parameters for tantalum isotopes, which were needed to calculate E1 γ-ray emission, were determined so as to reproduce the γ-ray spectrum at 500 keV. The presently evaluated cross sections are in good agreement with measurements. The data on ^{179,180m,182}Ta, which were missing in JENDL-4.0, were newly evaluated. The evaluated data are compiled into ENDF-formatted data files for the next release of JENDL general-purpose files.

Acknowledgemens

The author would like to thank the members of the Nuclear Data Center, JAEA, for their helpful comments on this work.

References

[1] Shibata K, Iwamoto O, Nakagawa T, Iwamoto N, Ichihara A, Kunieda S, Chiba S, Furutaka K, Otuka N, Ohsawa T, Murata T, Matsunobu H, Zukeran A, Kamada S, Katakura J. JENDL-4.0: A new library for nuclear science and engineering. J Nucl Sci Technol. 2011 Jan; 48:1-30.

[2] Chiba G, Okumura K, Sugino K, Nagaya Y, Yokoyama K, Kugo T, Ishikawa M, Okajima S. JENDL-4.0 benchmarking for fission reactor applications. J Nucl Sci Technol. 2011 Feb; 48:172-187.

[3] IAEA Safety Standards Series. Application of the concepts of exclusion, exemption and clearance (No. RS-G-1.7). Vienna: International Atomic Energy Agency; 2004.

[4] Shibata K, Nakagawa T, Asami T, Fukahori T, Narita T, Chiba S, Mizumoto M, Hasegawa A, Kikuchi Y, Nakajima Y, Igarasi S. Japanese evaluated nuclear data library, version-3 – JENDL-3 –. Tokai, Japan: Japan Atomic Energy Research Institute; 1990, JAERI 1319.

[5] Wang M, Audi G, Wapstra AH, Kondev FG, MacCormick M, Xu X, Pfeiffer B. The AME2012 atomic mass evaluation (II). Tables, graphs and references. Chinese Phys C. 2012 Dec; 36:1603-2014.

[6] Berglund M, Wieser ME. Isotopic compositions of the elements 2009. Pure Appl Chem. 2011 Feb; 83:397-410.

[7] Tuli JK. Nuclear wallet cards. 8th ed. Upton. NY: Brookhaven National Laboratory; 2011 Oct.

[8] Schumann M, Käppeler F. Neutron capture on ^{179}Ta. Phys Rev C. 1999 July; 60: 025802.

[9] Harvey JA, Hill NW, Mapoles ER, Level spacing and s-wave neutron strength function of ^{180}Ta + n. Oak Ridge: Oak Ridge National Laboratory; 1975, ORNL-5025, p.122-125.

[10] Stokes GE, Schuman RP, Simpson OD. The total neutron cross section of 115-day tantalum-182 from 0.01 to 1000 eV. Nucl Sci Eng. 1968; 33:16-23.

[11] Meaze AKM Moinul Haque, Devan K, Khandaker MU, Kim G, Son D, Lee YS, Kang H, Cho MH, Ko IS, Namkung W, Kim YA, Yoo KJ, Lee YY. Measurements of the neutron total cross-sections of tantalum by using pulsed neutrons based on an electron linac. J Korean Phy Soc. 2006 April; 48: 827-834.

[12] Mughabghab SF. Atlas of neutron resonances, resonance parameters and thermal cross sections Z = 1–100. Amsterdam: Elsevier; 2006.

[13] Kikuchi Y, Nakagawa T, Nakajima Y. ASREP: A computer program for automatic search of unresolved resonance parameters. Tokai, Japan: Japan Atomic Energy Research Institute; 1999, JAERI-Data/Code 99-025 [in Japanese].

[14] Iwamoto O. Development of a comprehensive code for nuclear data evaluation, CCONE, and validation using neutron-induced cross sections for uranium isotopes. J Nucl Sci Technol. 2007 May; 44:687-697.

[15] Akkermans JM, Gruppelaar H. Analysis of continuum gamma-ray emission in precompound-decay reactions. Phys Lett B. 1985 July; 157:95-100.

[16] Kunieda S, Chiba S, Shibata K, Ichihara A, Sukhovitskiĩ ESh. Coupled-channels optical model analyses of nucleon-induced reactions for medium and heavy nuclei in the energy region from 1 keV to 200 MeV. J Nucl Sci Technol. 2007 June;44:838–852.

[17] Tamura T. Analyses of the scattering of nuclear particles by collective nuclei in terms of the coupled-channel calculation. Rev Mod Phys. 1965 Oct;37:679–708.

[18] Koura H, Tachibana T, Uno M., Yamada M. Nuclidic mass formula on a spherical basis with an

improved even-odd term. Prog Theor Phys. 2005 Feb;113:305–325.

[19] Koning AJ, Delaroche JP. Local and global nucleon optical models from 1 keV to 200 MeV. Nucl Phys A. 2003;713:231–310.

[20] Lohr JM, Haeberli W. Elastic scattering of 9–13 MeV vector polarized deuterons. Nucl Phys A. 1974;232:381–397.

[21] Becchetti FD, Greenlees GW. A general set of ^{3}He and triton optical-model potentials for A > 40, E < 40 MeV. In: Barshall HH, Haeberli W, editors. Proceedings of the Third International Symposium on Polarization Phenomena in Nuclear Reactions; 1970 August 31 – September 4; Madison, Wisconsin: University of Wisconsin Press; 1971. p.682–683.

[22] Lemos OF. Elastic scattering of alpha-particles from 21 to 29.6 MeV in the nuclide region of Ti–Zn [dissertation]. (Orsay report, Series A., No. 136). Université de Paris-sud; 1972. French.

[23] Arthur ED, Young PG. Evaluated neutron-induced cross sections for ^{54,56}Fe to 40 MeV. Los Alamos: Los Alamos National Laboratory; 1980, LA-8626-MS.

[24] Capote R, Herman M, Obložinský P, Young PG, Goriely S, Belgaya T, Ignatyuk AV, Koning AJ, Hilaire S, Plujko VA, Avrigeanu M, Bersillon O, Chadwick MB, Fukahori T, Ge Z, Han Y, Kailas S, Kopecky J, Maslov VM, Reffo G, Sin M, Soukhovitskii ESh, Talou P. RIPL–reference input parameter library for calculations of nuclear reactions and nuclear data evaluations. Nucl Data Sheets. 2009 Dec;110:3107-3214.

[25] Gilbert A, Cameron AGW. A composite nuclear-level density formula with shell corrections. Can J Phys. 1965 Aug;43:1446–1496.

[26] Mengoni A, Nakajima Y. Fermi-gas model parametrization of nuclear level density. J Nucl Sci Technol. 1994 Feb;31:151-162.

[27] Myers WD, Swiatecki WJ. Nuclear masses and deformations. Nucl Phys. 1966 June;81:1–60.

[28] Voignier J, Joly S, Greiner G. Capture cross sections and gamma-ray spectra from the interaction of 0.5- to 3.0-MeV neutrons with nuclei in the mass range A = 63 to 209. Nucl Sci Eng. 1986; 93:43-56.

[29] Voignier J, Joly S, Greiner G. Corrigendum. Nucl Sci Eng. 1987; 96:343.

[30] Kopecky J, Uhl M, Chrien RE. Radiative strength in the compound nucleus ^{157}Gd. Phys Rev C. 1993 Jan; 47:312-322.

[31] Igashira M, Kitazawa H, Shimizu M, Komano H, Yamamuro N. Systematics of the pygmy resonance in keV neutron capture γ-ray spectra of nuclei with N $\approx$ 82–126. Nucl Phys A. 1986;457:301-316.

[32] Kopecky J. Gamma-ray strength functions. Vienna: International Atomic Energy Agency; 1998, IAEA-TECDOC-1034, 97-111.

[33] Möller P, Nix JR, Myers WD, Swiatecki WJ. Nuclear ground-state masses and deformations. Atom Data Nucl Data Tables. 1995; 59:185-381.

[34] Kopecky J, Uhl M. Test of gamma-ray strength functions in nuclear model calculations. Phys Rev C. 1990 May; 41:1941-1955.

[35] Koning AJ, Duijvestijn MC. A global pre-equilibrium analysis from 7 to 200 MeV based on the optical model potential. Nucl Phys A. 2004;744:15–76.

[36] Kalbach C. The Griffin model, complex particles and direct reactions. Z Phys A. 1977;283:401–411.

[37] Otuka N, Dupont E, Semkova V, Pritychenko B, Blokhin AI, Aikawa M, Babykina S, Bossant M, Chen G, Dunaeva S, Forrest RA, Fukahori T, Furutachi N, Ganesan S, Ge Z, Gritzay OO, Herman M, Hlavač S, Kato K, Lalremruata B, Lee YO, Makinaga A, Matsumoto K, Mikhaylyukova M, Pikulina G, Pronyaev VG, Saxena A, Schwerer O, Simakov SP, Soppera N, Suzuki R, Takács S, Tao X, Taova S, Tárkányi F, Varlamov VV, Wang J, Yang SC, Zerkin V, Zhuang Y. Towards a more complete and accurate experimental nuclear reaction data library (EXFOR): international collaboration between nuclear reaction data centres (NRDC). Nucl Data Sheets. 2014;120:272-276.

[38] Chadwick MB, Herman M, Obložinský P, Dunn ME, Danon Y, Kahler AC, Smith DL, Pritychenko B, Arbanas G, Arcilla R, Brewer R, Brown DA, Capote R, Carlson AD, Cho YS, Derrien H, Guber K, Hale GM, Hoblit S, Holloway S, Johnson TD, Kawano T, Kiedrowski BC, Kim H, Kunieda S, Larson NM, Leal L, Lestone JP, Little RC, McCutchan EA, MacFarlane RE, MacInnes M, Mattoon CM, McKnight RD, Mughabghab SF, Nobre GPA, Palmiotti G, Palumbo A, Pigni MT, Pronyaev VG, Sayer RO, Sonzogni AA, Summers NC, Talou P, Thompson IJ, Trkov A, Vogt RL, van der

Marck SC, Wallner A, White MC, Wiarda D, Young PG. ENDF/B-VII.1 nuclear data for science and technology: cross sections, covariances, fission product yields and decay data. Nucl Data Sheets. 2011 Dec;112:2887–2996.

[39] OECD Nuclear Energy Agency Data Bank. Available from http://www.oecd-nea.org/dbforms/data/eva/evatapes/jeff_32/

[40] Nakajima Y. JENDL activation cross section file. In: Igashira M, Nakagawa T, editors. Proceedings of the 1990 Symposium on Nuclear Data; 1990 November 29–30; Tokai. Tokai; Japan Atomic Energy Research Institute; 1991 (JAERI-M 91-032), p.43–57.

[41] Koning A, Forrest R, Kellet M, Mills R, Henriksson H, Rugama Y, editors. The JEFF-3.1 nuclear data library. Paris: OECD Nuclear Energy Agency; 2006 (JEFF Report 21).

[42] Wisshak K, Voss F, Arlandini C, Käppeler F, Heil M, Reifarth R, Krtička, Bečvář F. Stellar neutron capture on $^{180}Ta^{m}$. I. Cross section measurement between 10 keV and 100 keV. Phys Rev C. 2004; 69:055801.

[43] Cox SA. Neutron activation cross sections for Br^{79}, Br^{81}, Rh^{103}, In^{115}, I^{127}, and Ta^{181}. Phys Rev. 1964 Jan; 133:B378-B383.

[44] Frehaut J, Bertin A, Bois R, Jary J. Status of $(n, 2n)$ cross section measurements at Bruyeres-le-Chatel. Proceedings of Symposium on Neutron Cross-sections from 10 to 50 MeV; 1980 May 12-14; Upton, USA: Brookhaven National Laboratory; 1980. p.399-411.

[45] Vonach H, Pavlik A, Strohmaier B. Accurate determination of $(n, 2n)$ cross sections for heavy nuclei from neutron production spectra. Nucl Sci Eng. 1990; 106:409-414.

[46] Ashby VJ, Catron HC, Newkirk LL, Taylor CJ. Absolute measurement of $(n, 2n)$ cross sections at 14.1 MeV. Phys Rev. 1958 July; 111:616-621.

[47] Veeser LR, Arthur ED, Young PG. Cross sections for $(n, 2n)$ and $(n, 3n)$ reactions above 14 MeV. Phys Rev C. 1977 Nov; 16:1792-1802.

[48] Luo J, Tuo F, Kong X. Activation cross sections for reactions induced by 14 MeV neutrons on natural tantalum. Phys. Rev C. 2009 May;78:057603.

[49] Shibata K, Chiba G, Ichihara A, Kunieda S. Evaluation of neutron nuclear data on arsenic-75 for JENDL-4. J Nucl Sci Technol. 2010 Jan; 47:40-46.

Table 1 Isotopic abundances and reaction Q-values of tantalum isotopes.

	^{179}Ta	^{180m}Ta	^{181}Ta	^{182}Ta
E_x (keV)	0.0	77.1	0.0	0.0
Abundance(%)	1.82y*	0.01201	99.98799	114.74d*
Q-values (MeV)				
(n, γ)	6.648	7.654	6.063	6.934
(n, p)	0.888	1.705	-0.254	0.401
(n, α)	8.671	9.173	7.545	8.274
(n, d)	-2.986	-3.458	-3.724	-4.092
(n, t)	-4.355	-3.300	-4.855	-3.530
$(n, {}^3\mathrm{He})$	-4.834	-5.379	-6.241	-6.614
$(n, 2n)$	-7.830	-6.571	-7.577	-6.063
(n, np)	-5.211	-5.683	-5.949	-6.317
$(n, n\alpha)$	2.383	2.100	1.519	1.482
(n, nd)	-10.612	-9.557	-11.112	-9.787
$(n, 3n)$	-14.785	-14.401	-14.224	-13.640
$(n, 2np)$	-12.837	-11.782	-13.337	-12.012

* Half-lives are given for ^{179,182}Ta.

Table 2 Resolved and unresolved resonance regions.

Target nuclei	Resolved resonance	Unresolved resonance
^{179}Ta	–	3 eV – 100 keV
^{180m}Ta	10^{-5} eV – 103 eV	103 eV – 100 keV
^{181}Ta	10^{-5} eV – 2.4 keV	2.4 keV – 100 keV
^{182}Ta	10^{-5} eV – 34 eV	34 eV – 100 keV

Table 3 Thermal capture (C) and elastic scattering (E) cross sections in units of barns.

Target nuclei	Reaction	Present	JENDL-4.0	Mughabghab[12]
^{179}Ta	C	983.4	–	932±62
	E	7.740	–	–
^{180m}Ta	C	563.9	–	563±60
	E	3.850	–	–
^{181}Ta	C	20.68	20.68	20.5±0.5
	E	5.650	5.650	6.12±0.15
^{182}Ta	C	8295.0	–	8200±600
	E	31.76	–	–

Table 4 Optical model parameters for neutrons.

V_R^0	$= -34.40 - 6.18 \times 10^{-2}A + 3.37 \times 10^{-4}A^2 - 6.52 \times 10^{-7}A^3$ MeV
V_R^1	$= 0.027$
V_R^2	$= 1.2 \times 10^{-4}$ MeV^{-1}
V_R^3	$= 3.5 \times 10^{-7}$ MeV^{-2}
V_R^{DISP}	$= 94.88$ MeV
C_{viso}	$= 24.3$ MeV
λ_R	$= 1.05 \times 10^{-2} + 1.63 \times 10^{-4}V_R^0$ MeV^{-1}
W_D^{DISP}	$= 11.0$ MeV
WID_D	$= 12.72 - 1.54 \times 10^{-2}A + 7.14 \times 10^{-5}A^2$ MeV
C_{wiso}	$= 18.0$ MeV
λ_D	$= 0.0140$ MeV^{-1}
W_V^{DISP}	$= 34.0$ MeV
WID_V	$= 105.05 - 14.13 \times [1.0 + exp\{(A - 100.21)/13.47\}]^{-1}$ MeV
V_{SO}^0	$= 5.92 + 0.003A$ MeV
λ_{SO}	$= 0.005$ MeV^{-1}
W_{SO}^{DISP}	$= -3.1$ MeV
WID_{SO}	$= 160.0$ MeV
$R_{R,D,V}$	$= 1.21A^{1/3}$ fm
$a_{R,D,V}$	$= 0.49 + 3.22 \times 10^{-3}A - 2.07 \times 10^{-5}A^2 + 4.47 \times 10^{-8}A^3$ fm
R_{SO}	$= (1.18 - 0.65A^{-1/3})A^{1/3}$ fm
a_{SO}	$= 0.59$ fm

Table 5 Coupling schemes used in the interaction between neutron and target.

Target nuclei	Coupled levels*	Deformation parameters
^{179}Ta	$7/2^+(g.s.)$, $9/2^+(0.134)$, $11/2^+(0.295)$, $13/2^+(0.481)$	$\beta_2 = 0.25$ $\beta_4 = -0.03$
^{180m}Ta	$9^-(0.077)$, $10^-(0.280)$, $11^-(0.505)$	$\beta_2 = 0.25$ $\beta_4 = -0.04$
^{181}Ta	$7/2^+(g.s.)$, $9/2^+(0.136)$, $11/2^+(0.302)$, $13/2^+(0.495)$	$\beta_2 = 0.25$ $\beta_4 = -0.03$
^{182}Ta	$3^-(g.s.)$, $4^-(0.098)$, $5^-(0.173)$, $6^-(0.316)$	$\beta_2 = 0.24$ $\beta_4 = -0.05$

$*$ The number in the parentheses indicates the excitation energy in MeV.

Table 6 Level density parameters for each nucleus.

Nuclei	$a(*)$ 1/MeV	Δ MeV	E_{sh} MeV	T MeV	E_0 MeV	E_m MeV	$E_{level}^{highest}$ MeV
^{183}Ta	21.665	0.887	1.518	0.440	-0.207	3.986	0.971
^{182}Ta	21.566	0.000	1.177	0.446	-1.064	3.106	0.647
^{181}Ta	21.468	0.892	1.428	0.481	-0.603	4.644	0.773
^{180}Ta	21.369	0.000	1.388	0.471	-1.354	3.544	0.624
^{179}Ta	21.271	0.897	1.887	0.482	-0.700	4.735	0.891
^{178}Ta	21.172	0.000	1.749	0.394	-0.632	2.315	0.671
^{177}Ta	21.074	0.902	2.207	0.512	-1.128	5.326	0.497
^{182}Hf	21.566	1.779	1.735	0.491	0.056	5.820	1.173
^{181}Hf	21.468	0.892	1.438	0.470	-0.475	4.444	1.117
^{180}Hf	21.369	1.789	1.588	0.541	-0.532	6.736	1.630
^{179}Hf	21.271	0.897	1.623	0.499	-0.843	4.994	1.139
^{178}Hf	21.172	1.799	1.843	0.545	-0.608	6.823	1.651
^{177}Hf	21.074	0.902	1.769	0.519	-1.087	5.348	0.846
^{180}Lu	21.369	0.000	1.230	0.320	-0.071	1.276	0.562
^{179}Lu	21.271	0.897	1.638	0.440	-0.163	3.939	0.735
^{178}Lu	21.172	0.000	1.338	0.402	-0.633	2.367	0.475
^{177}Lu	21.074	0.902	1.751	0.488	-0.689	4.762	1.094
^{176}Lu	20.975	0.000	1.388	0.470	-1.281	3.445	0.709
^{175}Lu	20.876	0.907	1.723	0.528	-1.148	5.465	0.595

Table 7 E1 parameters for tantalum isotopes.

Resonance	$E_{0,i}$(MeV)	$\Gamma_{0,i}$(MeV)	$\sigma_{0,i}$(mb)
GDR	12.3	2.43	259.0
GDR	15.2	4.48	341.0
PR	5.5	2.5	3.0

Table 8 Gamma-ray strength functions for s-wave neutron in units of 10^{-4}.

Compound nuclei	Present work	Mughabghab[12]
^{180}Ta	522.0	–
^{181}Ta	121.2	500±40
^{182}Ta	111.8	145±5
^{183}Ta	178.2	231±128*

* Calculated from the s-wave average level-spacing and the s-wave average radiative width given in Ref.[12].

Table 9 Pre-equilibrium parameters.

Target nuclei	C_0 (n, n')	C_0 (n, p)	Knockout for (n, α)	Pickup for (n, α)	Pickup for (n, t)
^{179}Ta	1.0	1.0	1.0	1.1	2.5
^{180m}Ta	1.0	1.0	1.0	1.1	2.5
^{181}Ta	1.0	0.8	1.0	1.1	2.5
^{182}Ta	1.0	1.0	1.0	1.1	2.5

Figure Captions

Figure 1 Unresolved resonance region for n + ^{182}Ta.

Figure 2 Total cross section of elemental Ta.

Figure 3 Gamma-ray spectrum from n + ^{181}Ta at 500 keV.

Figure 4 Capture cross section of ^{180m}Ta.

Figure 5 Capture cross section of ^{181}Ta.

Figure 6 ^{181}Ta$(n,\gamma)^{182g+182m1}$Ta (G: $J^\pi = 3^-$, $T_{1/2}$=114.74 d; M1: $J^\pi = 5^+$, $T_{1/2}$=283 ms) reaction cross section. The 5^+ state is not regarded as meta stable in JENDL/A-96.

Figure 7 ^{181}Ta$(n,\gamma)^{182m2}$Ta ($J^\pi = 10^-$, $T_{1/2}$=15.84 m) reaction cross section.

Figure 8 ^{181}Ta$(n,2n)^{180}$Ta reaction cross section.

Figure 9 ^{181}Ta$(n,2n)^{180g}$Ta ($J^\pi = 1^+$, $T_{1/2} = 8.154$ h) reaction cross section.

Figure 10 ^{181}Ta$(n,3n)^{179}$Ta reaction cross section.

Figure 11 ^{181}Ta$(n,p)^{181}$Hf reaction cross section.

Figure 12 ^{181}Ta$(n,t)^{179}$Hf reaction cross section.

Figure 13 ^{181}Ta$(n,\alpha)^{178}$Lu reaction cross section.

Figure 14 ^{181}Ta$(n,np+d)^{180m}$Hf ($J^\pi = 8^-$, $T_{1/2} = 5.47$ h) reaction cross section.

Figure 15 Angular distributions of neutron scattered from ^{181}Ta.

Figure 16 Angle-integrated neutron emission spectra for ^{181}Ta.

Figure 17 Double-differential neutron emission spectra from ^{181}Ta at 14.1 MeV.

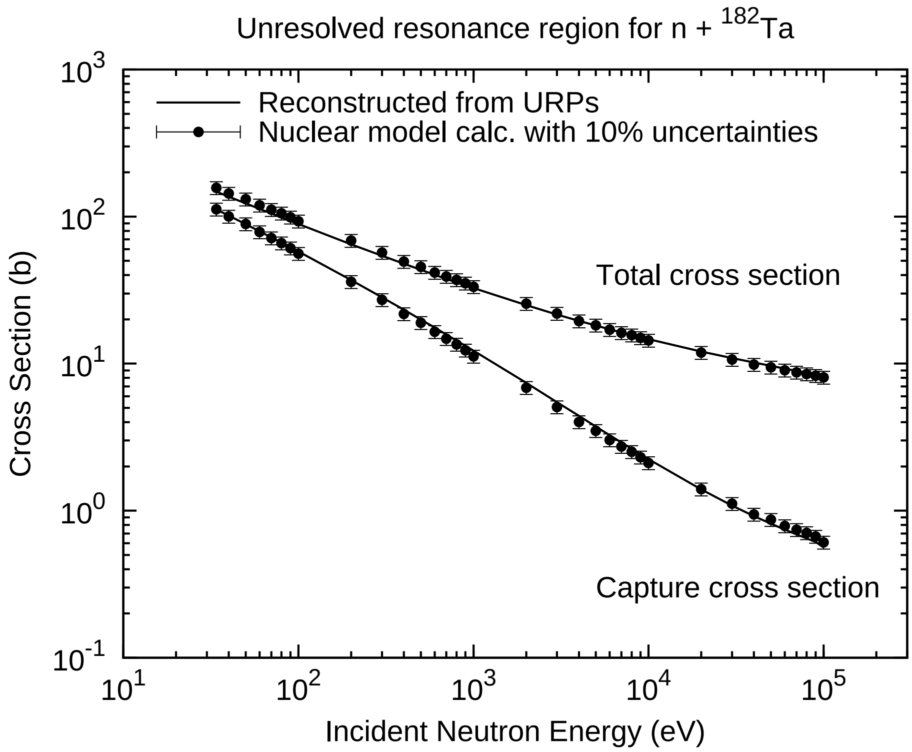

Figure 1 Unresolved resonance region for n + ^{182}Ta.

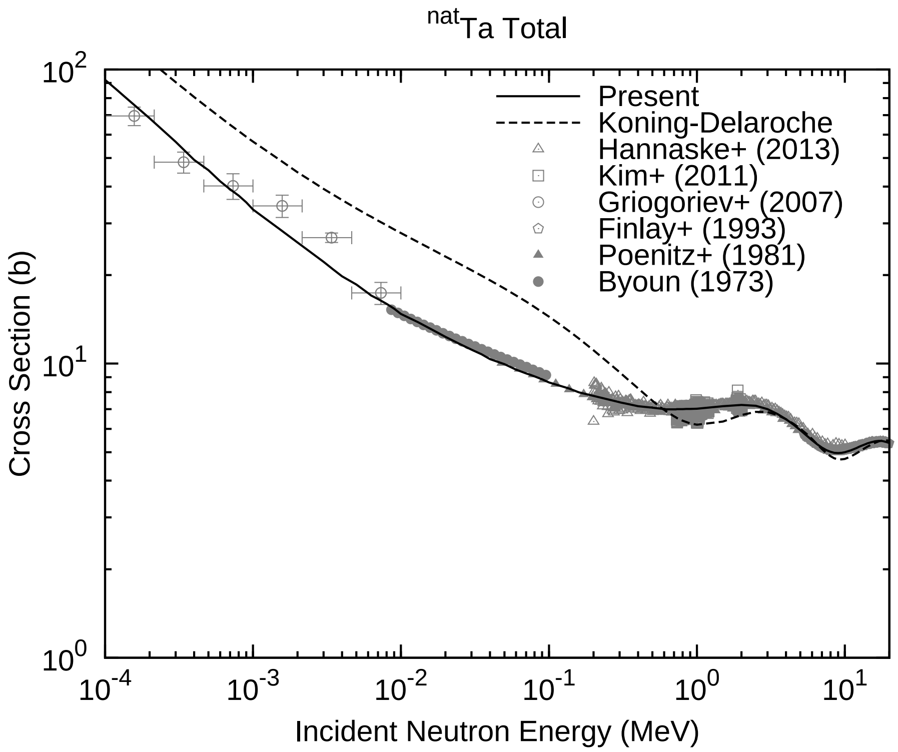

Figure 2 Total cross section of elemental Ta.

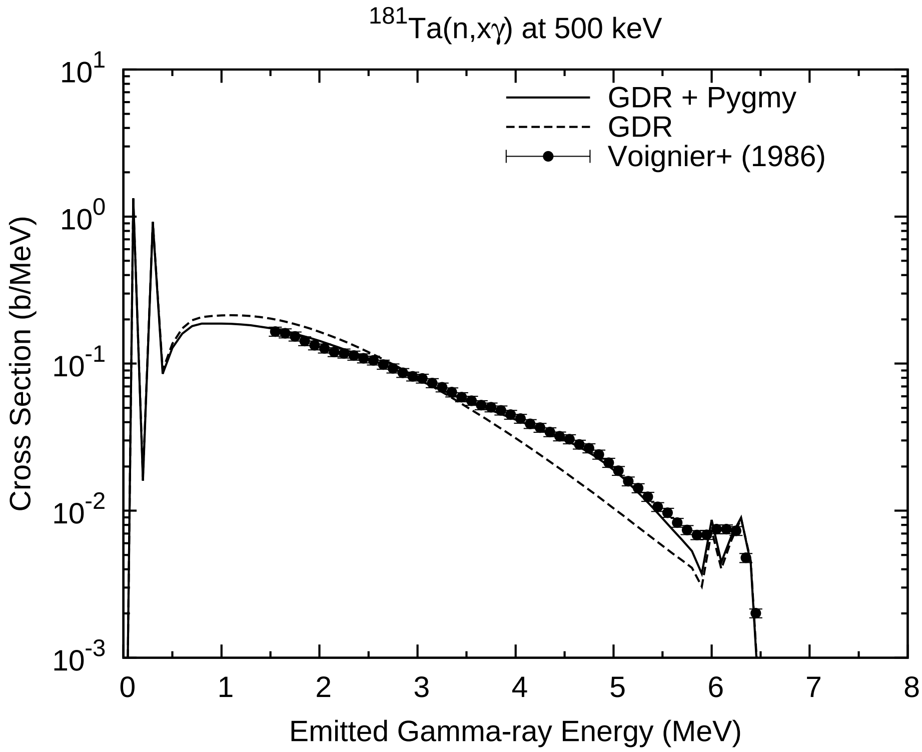

Figure 3 Gamma-ray spectrum from n + ^{181}Ta at 500 keV.

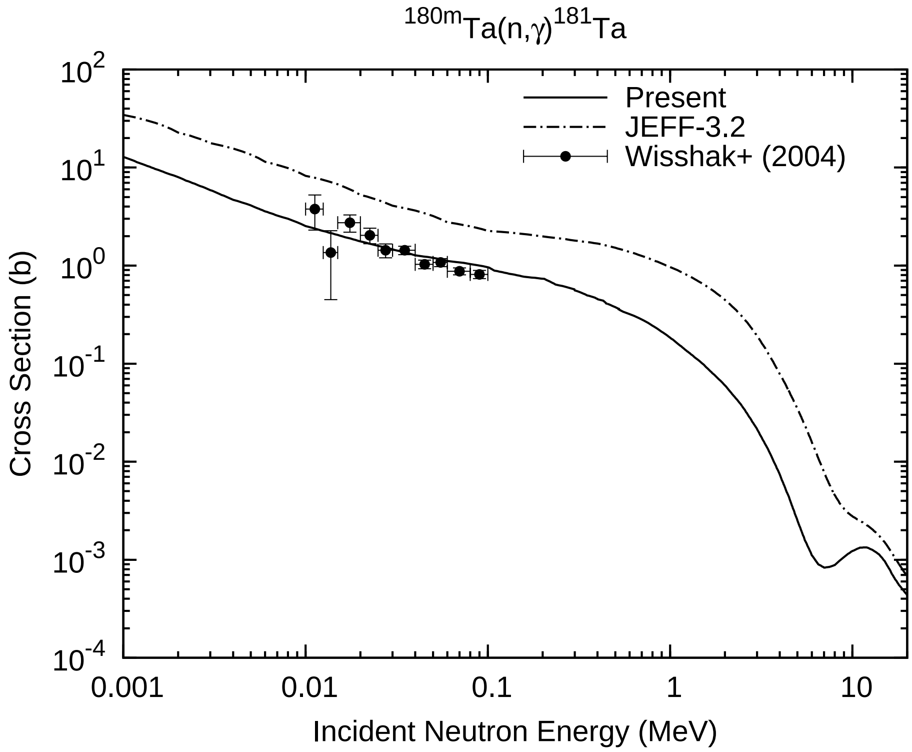

Figure 4 Capture cross section of ^{180m}Ta.

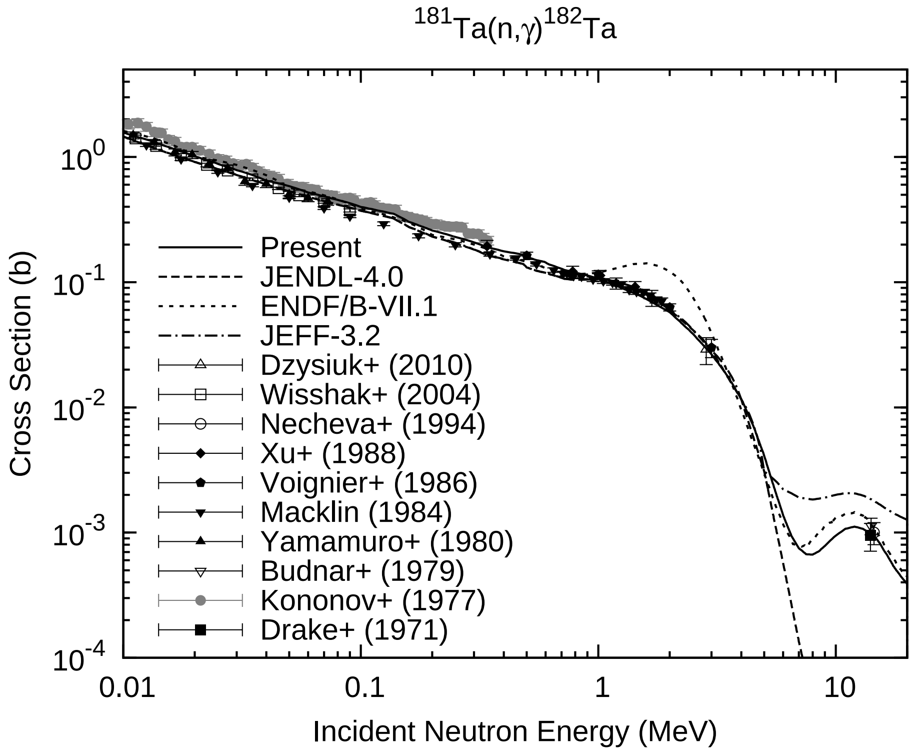

Figure 5 Capture cross section of ^{181}Ta.

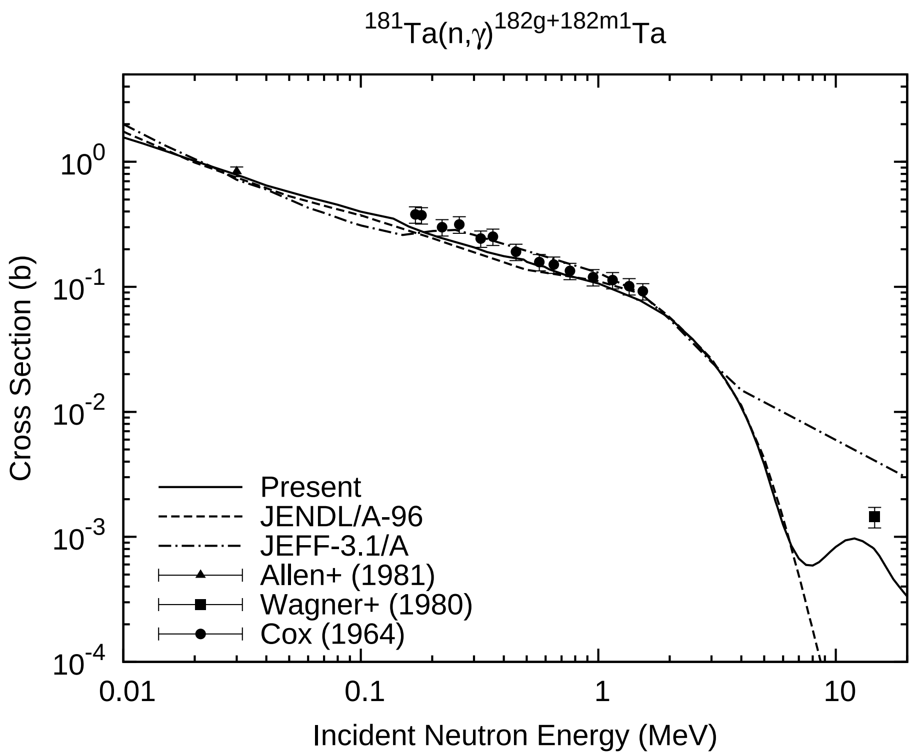

Figure 6 ^{181}Ta$(n,\gamma)^{182g+182m1}$Ta (G: $J^{\pi} = 3^{-}$, $T_{1/2}$=114.74 d; M1: $J^{\pi} = 5^{+}$, $T_{1/2}$=283 ms) reaction cross section. The 5^{+} state is not regarded as meta stable in JENDL/A-96.

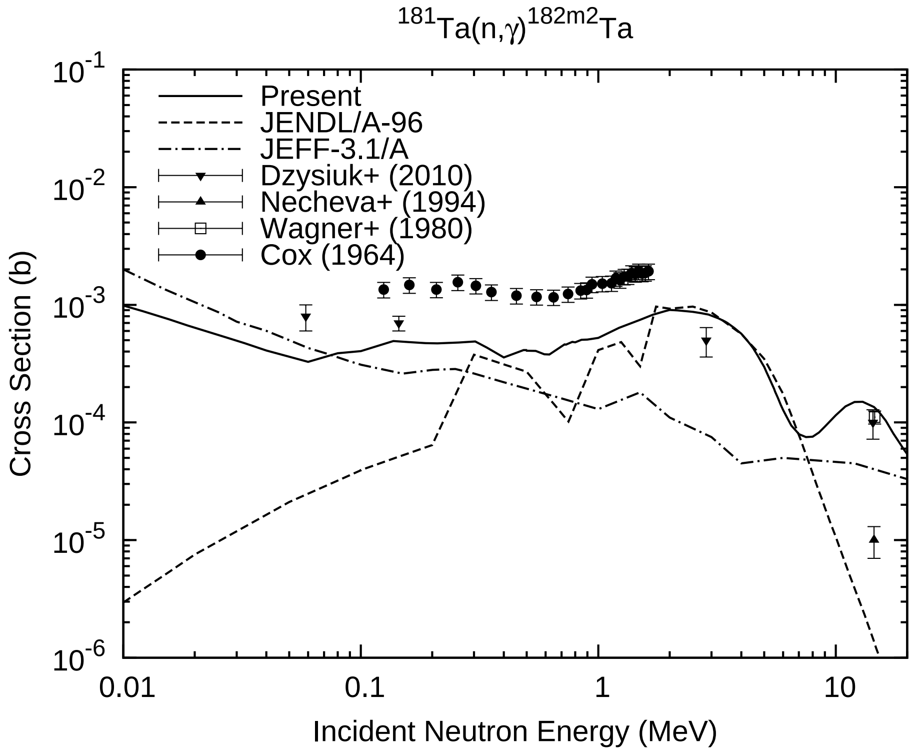

Figure 7 ^{181}Ta$(n,\gamma)^{182m2}$Ta ($J^{\pi} = 10^{-}$, $T_{1/2}$=15.84 m) reaction cross section.

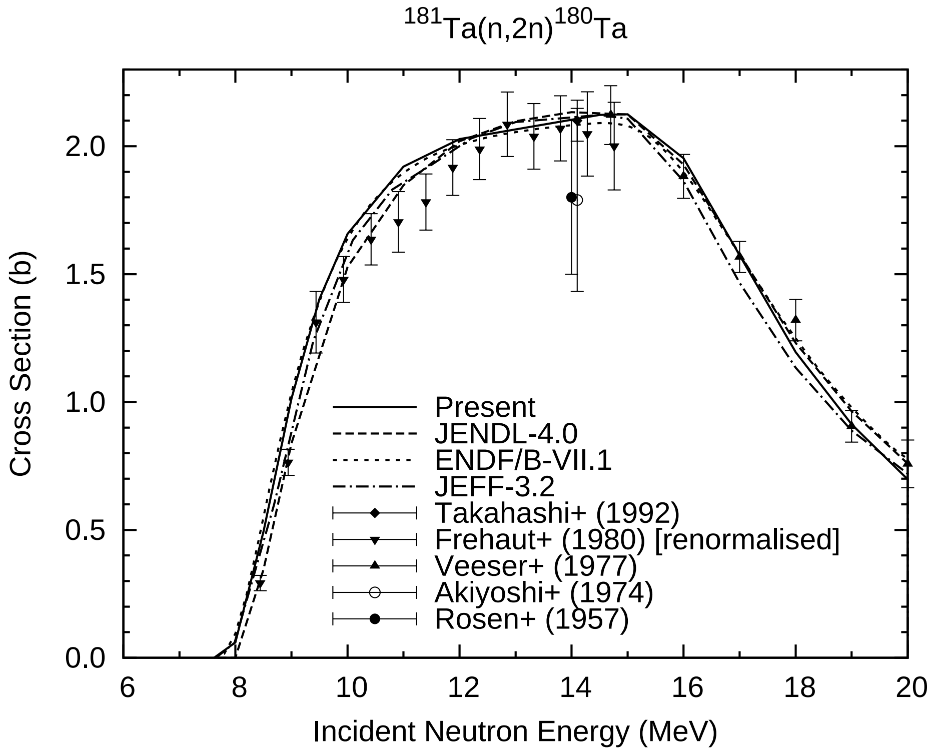

Figure 8 $^{181}\mathrm{Ta}(n,2n)^{180}\mathrm{Ta}$ reaction cross section.

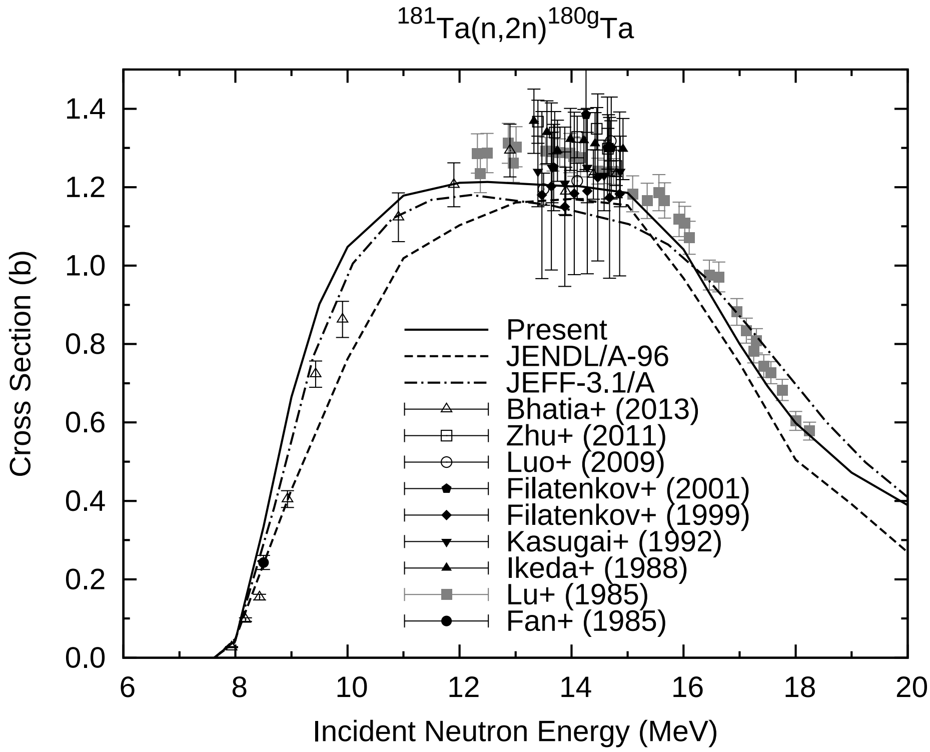

Figure 9 $^{181}\mathrm{Ta}(n,2n)^{180g}\mathrm{Ta}$ ($J^{\pi} = 1^{+}$, $T_{1/2} = 8.154$ h) reaction cross section.

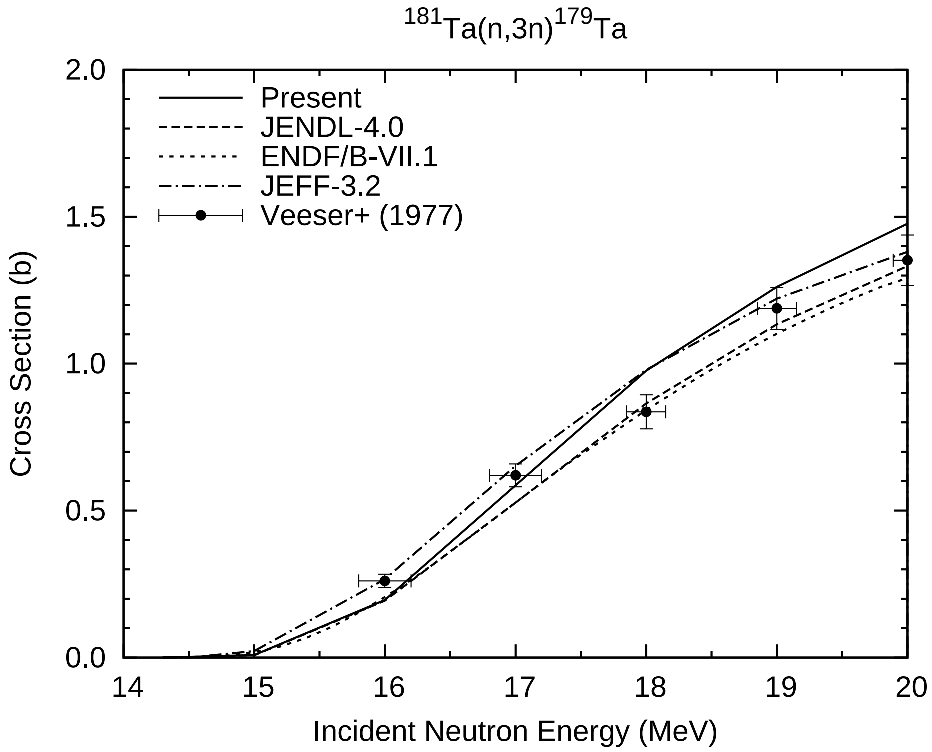

Figure 10 $^{181}\mathrm{Ta}(n,3n)^{179}\mathrm{Ta}$ reaction cross section.

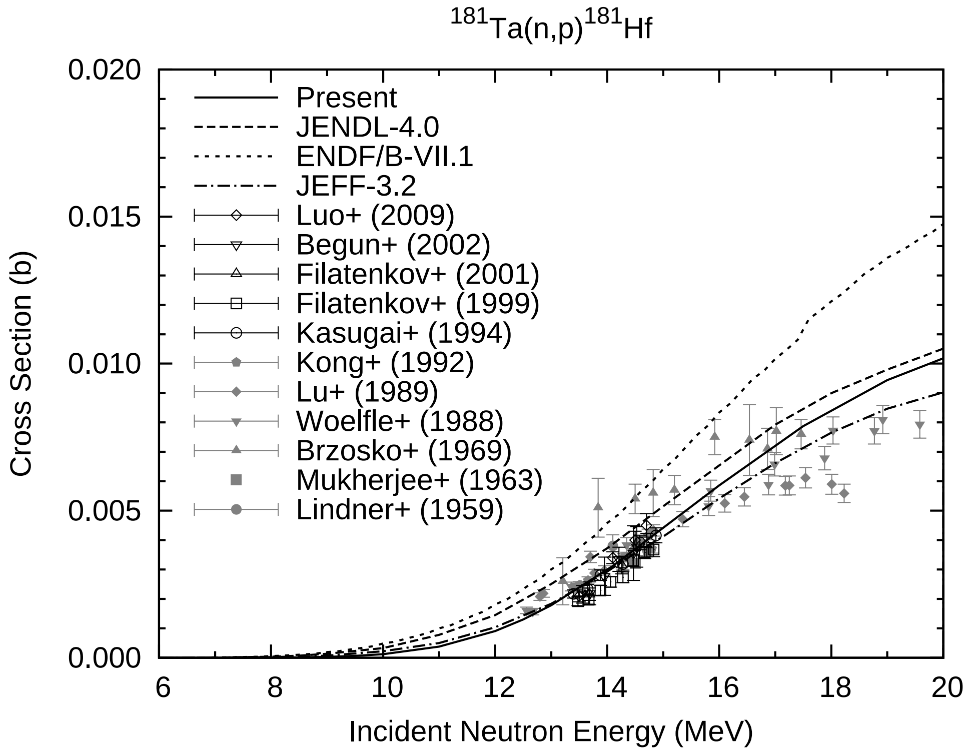

Figure 11 ^{181}Ta$(n,p)^{181}$Hf reaction cross section.

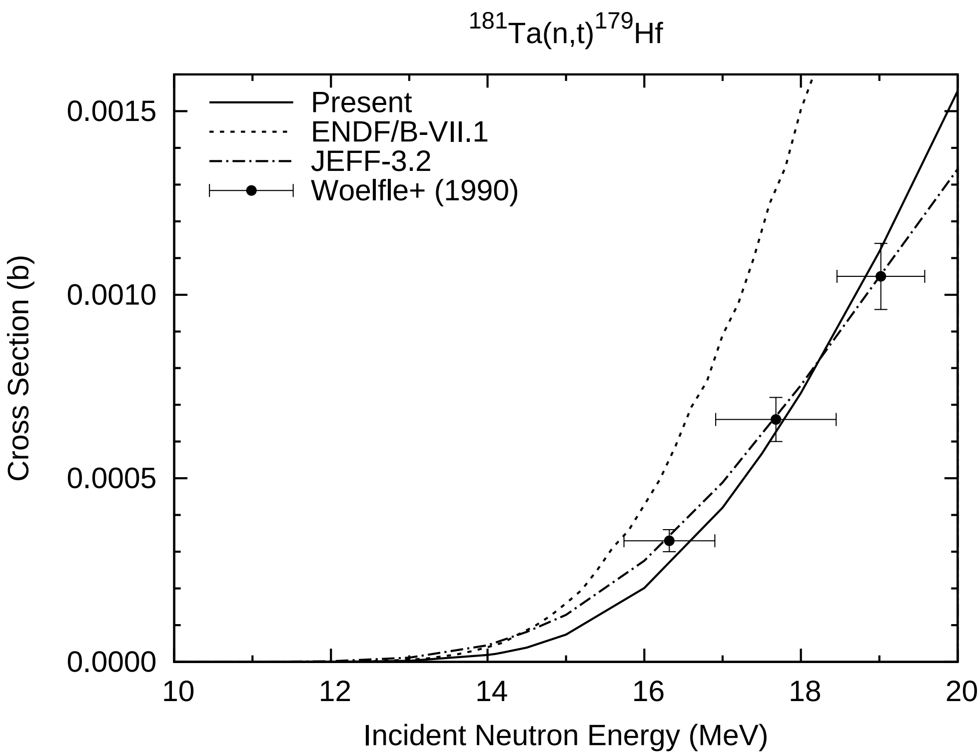

Figure 12 ^{181}Ta$(n,t)^{179}$Hf reaction cross section.

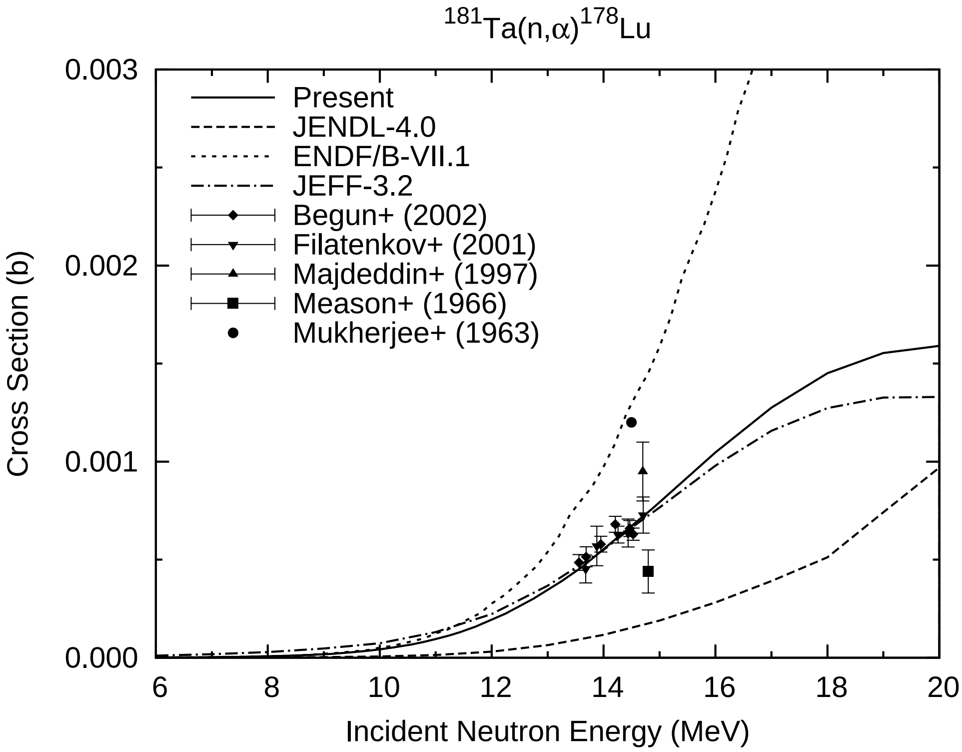

Figure 13 $^{181}\mathrm{Ta}(n,\alpha)^{178}\mathrm{Lu}$ reaction cross section.

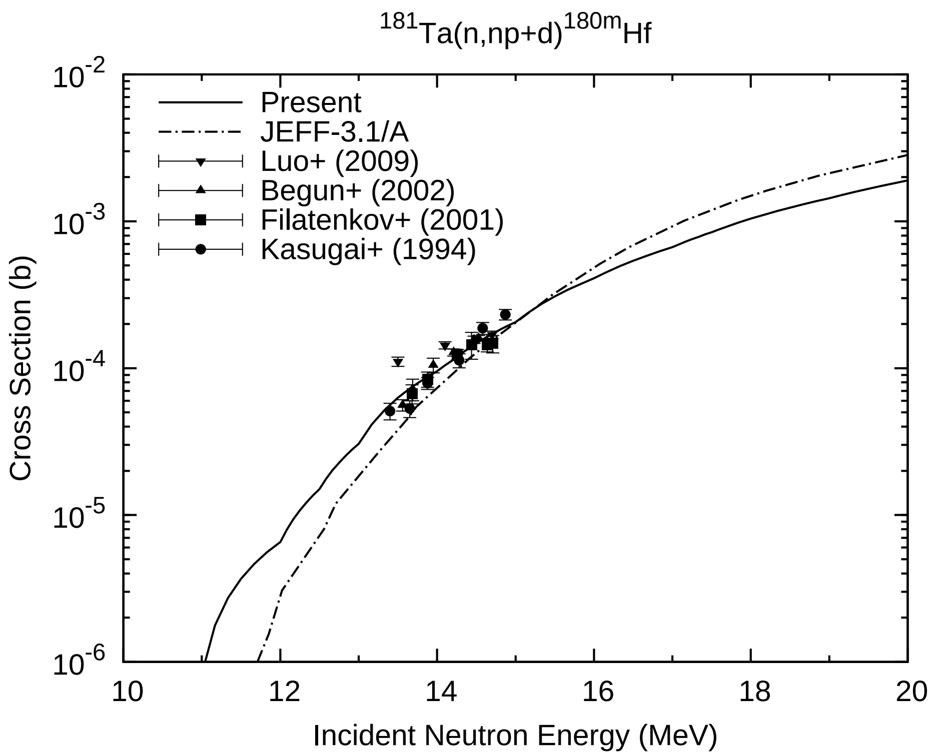

Figure 14 ^{181}Ta$(n, np + d)^{180m}$Hf ($J^{\pi} = 8^{-}$, $T_{1/2} = 5.47$ h) reaction cross section.

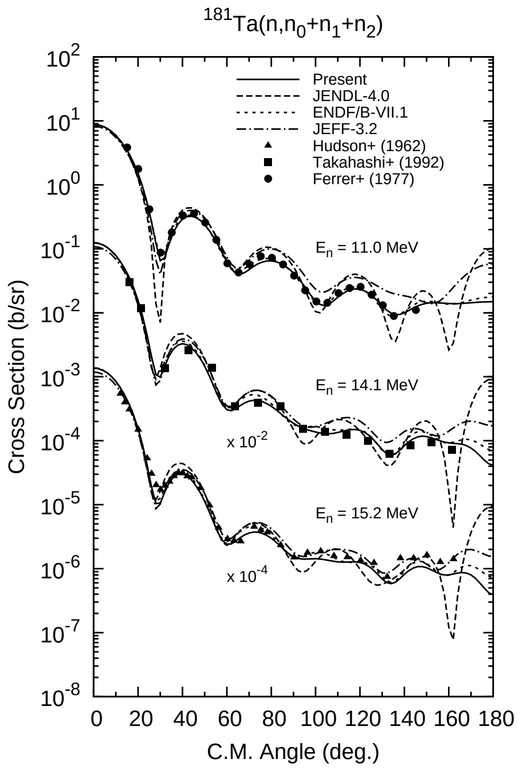

Figure 15 Angular distributions of neutron scattered from ^{181}Ta.

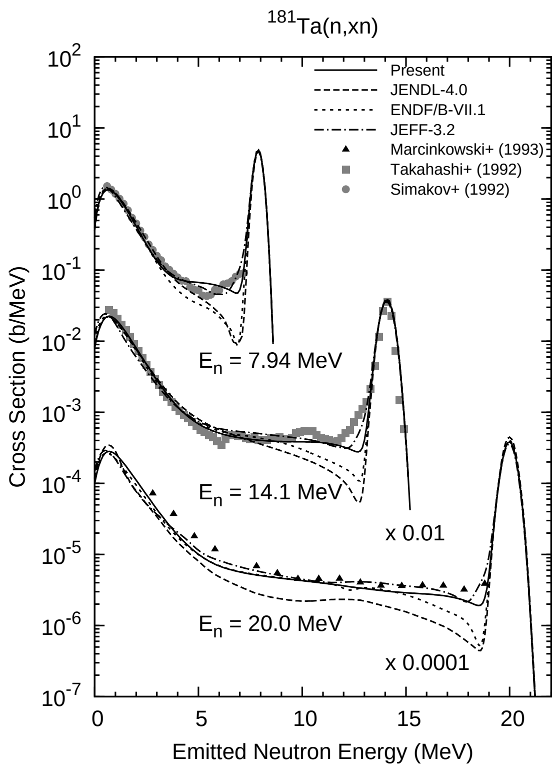

Figure 16 Angle-integrated neutron emission spectra for ^{181}Ta.

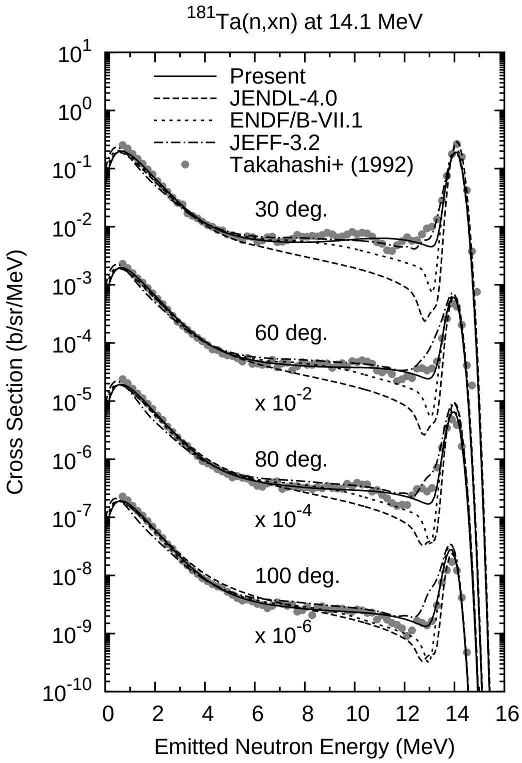

Figure 17 Double-differential neutron emission spectra from ^{181}Ta at 14.1 MeV.